Title	Multimodal MRI and multiomics reveal high-risk neurophenotype in brain-gut circuits as therapeutic target for Crohn's disease
Authors	Li, Xuehua;Zhang, Ruonan;Shen, Xiaodi;Lin, Shaochun;Wang, Chuhuai;Zheng, Weikai;Kong, Weimiao;Lin, Zihao;Li, Rongchang;Liu, Caiguang;Cao, Xin;Huang, Li;He, Weitao;Lin, Jinjiang;Wang, Haijie;Li, Zhoulei;Iacucci, Marietta;Ghosh, Subrata;Peng, Zhenpeng;Sun, Canhui;Chen, Minhu;Yang, Guang;Wang, Yejun;Mao, Ren;Feng, Shi Ting
Publication date	2026-04-03
Original Citation	Li, X, Zhang, R, Shen, X, Lin, S, Wang, C, Zheng, W, Kong, W, Lin, Z, Li, R, Liu, C, Cao, X, Huang, L, He, W, Lin, J, Wang, H, Li, Z, Iacucci, M, Ghosh, S, Peng, Z, Sun, C, Chen, M, Yang, G, Wang, Y, Mao, R & Feng, S T 2026, 'Multimodal MRI and multiomics reveal high-risk neurophenotype in brain-gut circuits as therapeutic target for Crohn's disease', Interdisciplinary Medicine, vol. 4, no. 4, e70122, pp. 1-20. https://doi.org/10.1002/inmd.70122
Type of publication	Article (Peer reviewed)
Link to publisher's version	10.1002/inmd.70122
Rights	cc_by
Download date	2026-08-28 05:52:58
Item downloaded from	https://hdl.handle.net/10468/19036

Received: 7 July 2025 | Revised: 6 March 2026 | Accepted: 19 March 2026

DOI: 10.1002/inmd.70122

RESEARCH ARTICLE

Interdisciplinary MEDICINE Open Access

Multimodal MRI and multiomics reveal high-risk neurophenotype in brain-gut circuits as therapeutic target for Crohn's disease

Xuehua Li[1] | **Ruonan Zhang**[1] | **Xiaodi Shen**[1] | **Shaochun Lin**[1] | **Chuhuai Wang**[2] | **Weikai Zheng**[1] | **Weimiao Kong**[3,4] | **Zihao Lin**[5] | **Rongchang Li**[5] | **Caiguang Liu**[5] | **Xin Cao**[3,4] | **Li Huang**[1] | **Weitao He**[1] | **Jinjiang Lin**[1] | **Haijie Wang**[6] | **Zhoulei Li**[1] | **Marietta Iacucci**[7] | **Subrata Ghosh**[7] | **Zhenpeng Peng**[1] | **Canhui Sun**[1,8] | **Minhu Chen**[5,9] | **Guang Yang**[6] | **Yejun Wang**[3,4] | **Ren Mao**[5] | **Shi-Ting Feng**[1]

[1]Department of Radiology, The First Affiliated Hospital of Sun Yat-Sen University, Guangzhou, China

[2]Department of Rehabilitation Medicine, The First Affiliated Hospital of Sun Yat-Sen University, Guangzhou, China

[3]Youth Innovation Team of Medical Bioinformatics, Shenzhen University Medical School, Shenzhen, China

[4]Department of Cell Biology and Genetics, College of Basic Medicine, Shenzhen University Medical School, Shenzhen, China

[5]Department of Gastroenterology, The First Affiliated Hospital of Sun Yat-Sen University, Guangzhou, China

[6]Shanghai Key Laboratory of Magnetic Resonance, East China Normal University, Shanghai, China

[7]APC Microbiome Ireland, College of Medicine and Health, University College Cork, Cork, UK

[8]Department of Radiology, Nansha Division, The First Affiliated Hospital of Sun Yat-Sen University, Guangzhou, China

[9]Department of Gastroenterology, Shenzhen Qianhai Taikang Hospital, Shenzhen, China

Correspondence

Xuehua Li and Shi-Ting Feng, Department of Radiology, The First Affiliated Hospital of Sun Yat-Sen University, 58 Zhongshan Road 2nd, Guangzhou 510080, China.

Email: lxueh@mail.sysu.edu.cn and fengsht@mail.sysu.edu.cn

Guang Yang, Shanghai Key Laboratory of Magnetic Resonance, East China Normal University, Dongchuan Road, Minhang District, Shanghai 200241, China.

Email: gyang@phy.ecnu.edu.cn

Yejun Wang, Youth Innovation Team of Medical Bioinformatics, Shenzhen University Medical School; Department of Cell Biology and Genetics, College of Basic Medicine, Shenzhen University Medical School, Shenzhen 518060, China.

Email: wangyj@szu.edu.cn

Ren Mao, Department of Gastroenterology, The First Affiliated Hospital, Sun Yat-Sen University, 58 Zhongshan Road 2nd, Guangzhou 510080, China.

Email: maor5@mail.sysu.edu.cn

Xuehua Li, Ruonan Zhang, Xiaodi Shen, Shaochun Lin, and Chuhuai Wang contributed equally to this work.

Funding information
National Natural Science Foundation of China, Grant/Award Numbers: 82572164, 82270693, 82471948, 82271958, 82072002, 82070680, 82222010; Basic and Applied Basic Research Foundation of Guangdong Province, Grant/Award Numbers: 2023B1515020070, 2023A1515011097, 2026A1515012338; National Key Research and Development Program of China, Grant/Award Number: 2023YFC2507300; Key Area Research and Development Program of Guangdong Province, Grant/Award Number: 2023B1111040003; Fundamental Research Funds for the Central Universities, Sun Yat-sen University, Grant/Award Number: 24ykqb003; 2023 SKY Imaging Research Fund of the Chinese International Medical Foundation, Grant/Award Number: Z-2014-07-2301

Abstract

The brain-gut axis shapes Crohn's disease (CD) pathogenesis, yet CD-associated neurophenotypes lack defined clinical and mechanistic significance. This work aimed to define these neurophenotypes, assess their prognostic impact, elucidate neurophenotype-driven progression mechanisms using multi-omics, and validate their therapeutic potential in vivo. 109 CD patients were prospectively recruited from two centers and underwent baseline multimodal neuro-MRI, MR enterography, ileocolonoscopy, and fecal/blood sample collection. The neurophenotypes were characterized using a multimodal neuro-MRI model developed from 13 of 13,870 features. 83 patients were followed up for disease progression, with repeated brain-gut assessments. Multi-omics (fecal microbiome/metabolomics, serum metabolomics/neurotransmitters) were used to decode the mechanisms underlying neurophenotype-driven progression. Dextran sulfate sodium (DSS)-induced colitis mice with different neurophenotypes were treated with repeated transcranial magnetic stimulation (rTMS) to explore its therapeutic potential. Multimodal neuro-MRI accurately mapped CD-specific neural signatures, stratifying patients into high-risk (neurophenotype score ≥ 0.45) and low-risk neurophenotypes with robust cross-center validity (training cohort AUC = 0.842, test cohort AUC = 0.824). High-risk neurophenotype was identified as an independent predictor of accelerated disease progression (Hazard ratio = 15.46, $p = 0.030$), independent of intestinal inflammation. Integrated multi-omics revealed that the high-risk neurophenotype contributed to CD progression through microbial-metabolic-neurotransmitter networks where tryptophan emerged as the central regulatory hub. Serum tryptophan levels were negatively correlated with neurophenotype severity and intestinal disease progression. rTMS targeting high-risk neurophenotype in DSS-induced colitis mice elevated tryptophan levels and ameliorated intestinal disease activity. This study redefines the high-risk neurophenotype as a sustained pathogenic driver rather than a mere phenomenon, proposing brain-gut axis modulation as a promising therapeutic strategy distinct from conventional anti-inflammatory approaches.

KEYWORDS
Crohn's disease, intestinal disease progression, multimodal MRI, neurophenotype

1 | INTRODUCTION

Crohn's disease (CD) is a lifelong and disabling inflammatory bowel disease.[1] Despite the introduction of advanced therapies, including biologics and small-molecule therapies, many patients exhibit suboptimal responses.[2] Extraintestinal manifestations, particularly neurological involvement, are increasingly recognized as contributors to disease burden.[3] However, current clinical management centers on intestinal inflammation, neglecting neurological dysfunction's impact on treatment efficacy; this contributes to treatment failure in some patients due to persistent extraintestinal neurological burden. Investigating the brain-gut axis in CD could uncover novel mechanisms underlying treatment failure and guide dual-target therapies addressing intestinal and neurological pathology.

Although the brain-gut axis in CD has gained attention,[3,4] critical gaps remain. First, while magnetic resonance imaging (MRI) is the optimal tool to characterize neural alterations in CD, most studies rely on single-modal neuroimaging,[5,6] lacking integration of multimodal data to comprehensively map brain-gut interactions. Second, neurological dysfunction's independent prognostic value remains unclear. Third, mechanisms linking neurological dysfunction to disease progression are also undefined.

Furthermore, neuro-targeted therapies' gut benefits are unproven. Addressing these gaps is essential to unravel the role of brain-gut axis in CD and advance therapeutic strategies targeting this pathway.

Therefore, this prospective study aimed to: (1) Define CD neurophenotypes using multimodal neuro-MRI; (2) Investigate their independent impact on CD progression during longitudinal follow-up; (3) Elucidate mechanisms underlying neurophenotype-driven disease progression through integrated multi-omics analysis, revealing key mediators within this brain-gut network; and (4) Explore therapeutic potential of targeting neurological abnormalities to ameliorate intestinal inflammation in vivo, with outcomes assessed via key mediators. By integrating advanced neuroimaging, multi-omics, and neuromodulation interventions, we enhance understanding the brain-gut axis's role in CD and highlight its potential as a risk-stratified biomarker and therapeutic target.

2 | MATERIALS AND METHODS

2.1 | Human participants

From June 2021 to May 2023, 113 CD patients were recruited from two centers. Inclusion criteria: (a) Aged 18–45 years; (b) Completion of multimodal neuro-MRI and psychological questionnaires[7–9]; and (c) MR enterography (MRE), ileocolonoscopy, and blood/fecal sample collection within one week of brain MRI. Exclusion criteria: (a) Recent (<3 months) use of antibiotics or central nervous system drugs; (b) History of neurosurgery, cerebrovascular disease, or brain trauma with loss of consciousness; or (c) Presence of brain lesions or metal implants on MR scan (Supporting Information S1: Figure S1, Table 1). Patients participating in the follow-up study were further required to have at least 12 months of follow-up without disease progression and complete follow-up data. Moreover, we enrolled 25 healthy controls (HCs; male/female = 20/5; mean age: 29.28 ± 6.30 years) to contribute to brain MRI (Supporting Information S1). All participants completed the State-Trait Anxiety Inventory (STAI),[7] Perceived Stress Scale (PSS),[8] and Beck Depression Inventory (BDI)[9] (Supporting Information S1).

2.2 | Using multimodal neuro-MRI to define CD neurophenotypes

Of 113 patients, four with unexpected brain lesions were excluded, leaving 109 patients whose MRI data were used for neurophenotype modeling. Of these, 77 (male/female = 67/10) from Center 1 constituted the training cohort and 32 (male/female = 27/5) from Center 2 formed the test cohort.

2.2.1 | Assessing intestinal inflammation severity

Intestinal inflammation was evaluated using MRE (Supporting Information S1) and ileocolonoscopy. MRE-derived indices, magnetic resonance index of activity (MaRIA)[10] and magnetic resonance enterography global score (MEGS)[11] quantified intramural/extramural lesions. Simplified endoscopic activity score for Crohn's disease (SES-CD)[12] scored mucosal lesions. Moderate-to-severe inflammation was defined by ≥ 2 criteria: (1) MaRIA ≥ 11[13]; (2) MEGS ≥ 10 for small bowel or MEGS ≥ 12 for colon[14,15]; or (3) SES-CD ≥ 11.[16,17] Others were categorized as no-to-mild inflammation (Supporting Information S1). Overall, 55 of 109 patients exhibited moderate-to-severe inflammation while 54 had no-to-mild inflammation.

2.2.2 | Acquisition of brain MRI

All patients underwent 3.0T brain MRI, including T1-weighted imaging (T1WI), diffusion spectrum imaging (DSI), resting-state blood-oxygen-level-dependent (BOLD) imaging, arterial spin labeling (ASL), and quantitative susceptibility mapping (QSM) (Supporting Information S1: Table S1).

2.2.3 | Data preprocessing, brain region segmentation, and feature extraction

MRI data were processed to generate 29 quantitative parameter maps. T1WI images were automatically segmented into 95 brain regions using the FreeSurfer toolbox,[18] with all maps co-registered to T1WI. Five descriptors (mean, standard deviation [std], 10th/50th/90th percentile [p10/p50/p90]) were extracted per brain region per map. 13,775 features (5 features × 29 parameter maps × 95 brain regions) and 95 relative volume (vol) of the brain region were obtained, yielding 13,870 features per patient (Supporting Information S1).

2.2.4 | Neurophenotype characterization model development

A three-step strategy with logistic regression was used to identify significant neuroimaging features for developing

TABLE 1 The baseline characteristics of the study cohort.

	Total (n = 109)	No-mild inflammation (n = 54)	Moderate-severe inflammation (n = 55)	p value
Clinical variables				
Sex, n (male/female)	94/15	43/11	51/4	0.049
Age, years (mean ± SD)	29.31 ± 7.08	28.85 ± 6.91	29.76 ± 7.29	0.5
Education[a] (median [IQR])	4 (4–5)	4 (4–5)	5 (4–5)	0.29
Smoking history, n (%)	13 (11.93%)	3 (5.56%)	10 (18.18%)	0.05
Alcohol history, n (%)	13 (11.93%)	5 (9.26%)	8 (14.55%)	0.44
BMI (kg/m^2) (mean ± SD)	20.15 ± 3.35	20.25 ± 3.16	20.05 ± 3.56	0.75
Psychological scales				
S-score (mean ± SD)	41.66 ± 10.26	41.80 ± 9.82	41.53 ± 10.77	0.89
T-score (mean ± SD)	43.06 ± 9.95	42.83 ± 8.81	43.29 ± 11.10	0.81
BDI (mean ± SD)	11.03 ± 9.45	10.89 ± 8.82	11.16 ± 10.11	0.88
PSS (mean ± SD)	37.19 ± 7.91	37.57 ± 7.76	36.82 ± 8.11	0.62
Neurophenotype score	0.48 ± 0.31	0.30 ± 0.23	0.66 ± 0.27	<0.001
Disease traits				
Disease duration, months (median [IQR])	48 (18–101.5)	58.50 (24–105.75)	36 (12–96)	0.52
Score of abdominal pain[b] (median [IQR])	3 (1–5)	2 (1–5)	3 (2–5)	0.08
CDAI, n (%)				0.04
Remission (<150)	40 (36.70%)	25 (46.30%)	15 (27.27%)	
Mild disease (150–220)	28 (25.69%)	13 (24.07%)	15 (27.27%)	
Moderate disease (220–450)	41 (37.61%)	16 (29.63%)	25 (45.45%)	
Severe disease (>450)	0	0	0	
Disease location, n (%)				0.997
L1 (terminal ileum ± caecum)	19 (17.43%)	9 (16.67%)	10 (18.18%)	
L2 (colonic)	4 (3.67%)	3 (5.56%)	1 (1.82%)	
L3 (ileocolic)	83 (76.15%)	40 (74.07%)	43 (78.18%)	
L4 (upper gastrointestinal tract)	3 (2.75%)	2 (3.70%)	1 (1.82%)	
Disease behavior, n (%)				0.001
Non-stricturing, non-penetrating	48 (44.04%)	32 (59.26%)	16 (29.09%)	
Intestinal stricture	46 (42.20%)	19 (35.19%)	27 (49.09%)	
Intestinal penetration	15 (13.76%)	3 (5.55%)	12 (21.82%)	
Perianal diseases, n (%)				0.09
None	37 (33.94%)	22 (40.74%)	15 (27.27%)	
Perianal fistula	60 (55.05%)	28 (51.85%)	32 (58.18%)	
Perianal abscess	12 (11.01%)	4 (7.41%)	8 (14.55%)	
Inflammation scores				
MaRIA (mean ± SD)	17.12 ± 11.33	10.03 ± 9.35	24.08 ± 8.44	<0.001
MEGS (mean ± SD)	12.24 ± 10.35	5.65 ± 4.88	18.71 ± 10.23	<0.001

TABLE 1 (Continued)

	Total (n = 109)	No-mild inflammation (n = 54)	Moderate-severe inflammation (n = 55)	p value
SES-CD (median [IQR])	6 (0–10)	3 (0–9)	6 (2–15)	0.02
Inflammation degree (BI0/BI1)	54/55	N/A	N/A	N/A
Laboratory results				
CRP (mg/L) (median [IQR])	23 (9–40.5)	3.22 (0.80–25.13)	16.40 (3.81–36.90)	<0.05
ESR (mm/h) (mean ± SD)	29.58 ± 25.54	22.80 ± 22.42	36.24 ± 26.84	<0.01
HB (g/L)	126.91 ± 21.46	130.50 ± 18.06	123.40 ± 24.00	0.08
ALB (g/L)	38.04 ± 7.27	39.60 ± 9.12	36.50 ± 4.40	0.03
Drug use[c], n (%)				
Biologics	28 (25.69%)	15 (27.78%)	13 (23.64%)	0.50
Corticosteroids	7 (6.42%)	3 (5.56%)	4 (7.27%)	0.51
Immunomodulator	36 (33.02%)	20 (37.04%)	16 (29.09%)	0.42
5-Aminosalicylic acid	22 (20.18%)	9 (16.67%)	13 (23.64%)	0.43

Note: Continuous variables: mean ± SD (normally distributed) or median [IQR] (non-normal); Categorical data: n (%).

Abbreviations: ALB, albumin; BDI, beck depression inventory; BI0, none-to-mild inflammation; BI1, moderate-to-severe inflammation; BMI, body mass index; CD, Crohn's disease; CDAI, Crohn's disease activity index; CRP, C-reactive protein; ESR, erythrocyte sedimentation rate; HB, hemoglobin; IQR, interquartile range; MaRIA, Magnetic Resonance Index of Activity; MEGS, Magnetic Resonance Enterography Global Score; PSS, perceived stress scale; SD, standard deviation; SES-CD, Simplified Endoscopic Activity Score for Crohn's disease; S-score, state score of State-Trait Anxiety Inventory; T-score, trait score of State-Trait Anxiety Inventory.

[a]Education level graded 1–6: 1 = Primary; 2 = Junior High; 3 = Senior High; 4 = Junior College; 5 = Undergraduate; 6 = Postgraduate.

[b]Abdominal pain severity assessed via 0–10 Visual Analog Scale (0 = no pain; 10 = worst pain).

[c]Medicine use within 3 months before inclusion.

neurophenotype characterization model (Supporting Information S1). This model quantified neurophenotype distinctions between intestinal inflammation subgroups. Its robustness was ensured through fivefold cross-validation in the training cohort, ultimately selecting 13 discriminative features.

The model's simplified formulation is:

$$\text{sigmoid}\left(\left(\sum_{k=0}^{n}\text{FeatureK} * \text{Coef}\right) + \text{bias}\right),$$

where "FeatureK" is the value of kth brain feature retained in model, "Coef"are the values generated by model for each brain feature, and "bias" is the bias value of linear regression (Supporting Information S1). The model performance was validated in an external test cohort using a receiver operating characteristic (ROC) curve (AUC). Model interpretation was conducted using SHapley Additive exPlanations (SHAP)[19] through the Python libraries SciPy and scikit-learn. Optimal classification threshold of neurophenotype score was determined based on the Youden index.

2.3 | Investigating independent impact of CD neurophenotypes on intestinal disease progression

2.3.1 | Disease progression definition

Disease progression was defined by meeting ≥ 1 criteria[3,20] (Supporting Information S1): (1) new penetrating diseases; (2) new stricture/obstruction; (3) progressive perianal disease; (4) CD-related surgery; or (5) CD-related hospitalization. Follow-up endpoint was defined as the time of disease progression or the end of follow-up for progression-free patients.

Among 109 patients, 26 with baseline strictures or penetrating diseases were excluded; the remaining 83 patients (male/female = 70/13) were followed up with an average period of 42 ± 24 weeks. This sample size exceeds the 55 patients required by an a priori G*Power (v3.1.9.7) analysis, which used pilot data (n = 25, r = 0.459) and parameters (α = 0.05, power = 0.95, two-tailed) to ensure sufficient power for assessing the neurophenotype-progression association.

2.3.2 | Impact of neurophenotype on disease progression

To investigate neurophenotype-specific contributions to disease progression, we analyzed data from 83 followed-up patients. Baseline patient stratification by inflammation severity (no-to-mild/moderate-to-severe) and neurophenotype scores (low/high) enabled progression comparisons within matched inflammation strata, decoupling neurophenotype-specific effects. Neuroimaging ($n = 15$) and psychological assessments ($n = 83$) with inflammation evaluation ($n = 83$) were repeated, revealing differences in brain and gut trajectory. Cox regression (univariate/multivariate) and Kaplan-Meier method with log-rank tests were used to investigate neurophenotypes' independent prognostic value. Ultimately, neurophenotypes associations with MRE abnormalities (Supporting Information S1) and progression were analyzed to validate these brain-gut axis interactions.

2.4 | Elucidating links between neurophenotypes and disease progression via integrated multi-omics

To dissect this brain-gut interaction mechanisms, we performed multi-omics profiling on baseline blood ($n = 105$) and fecal ($n = 70$) samples from CD patients. Fecal microbiome (16S rRNA gene amplicon/metagenomic sequencing), targeted metabolomics (184 fecal and 470 blood metabolites), and 19 blood neurotransmitters were tested. The relationships among neurophenotypes, multi-omics profiling, and intestinal inflammation/outcomes were analyzed. Beyond conventional mediation analysis, we employed a novel principal component (PC3) Analysis-coupled Mediation Analysis (PCMA)[21] to delineate causal pathways. Sample collection, multi-omics testing and data analysis are detailed in Supporting Information S1.

2.5 | Neurophenotype-targeted treatment for alleviating intestinal inflammation in vivo

2.5.1 | Animal model

Male C57BL/6 mice (8-week-old; GemPharmatech Co., Ltd) were used to establish dextran sulfate sodium (DSS)-induced colitis (2.25% DSS, days 1–7; water, days 8–10).[22] Disease activity index (DAI)[23] was monitored daily. DSS-induced colitis triggers depressive-like behaviors in some mice.[24,25] Considering clinical correlations between high-risk neurophenotype and depressive symptoms in CD patients, we conducted behavioral tests (sucrose preference and open-field assays) to identify mice with depression-like behaviors,[26] simulating patients' high-risk neurophenotype. Sucrose preference was measured over 24 h on day 11, and open-field testing was performed on day 12. Mice positive in both tests were classified as high-risk neurophenotype (Group 1, G1), others as low-risk (Group 2, G2). Moreover, a subgroup of mice administered saline served as healthy controls (Group 3, G3). Animal modeling details are shown in Supporting Information S1.

2.5.2 | Neurophenotype-targeted treatment using repetitive transcranial magnetic stimulation (rTMS)

After establishing G1, G2, and G3 models, mice in each group were randomly divided into three subgroups to receive 0, 5, or 10 days of rTMS using an animal coil (YIRUIDE Y064, YIRUIDE Company) for daily treatment of neuropsychiatric disorder (Supporting Information S1).

2.5.3 | Samples collection and testing

Both fecal and serum samples were collected pre- and post-treatment and stored at −80°C. Serum samples were analyzed for S100β (blood-brain barrier permeability),[27] tryptophan (brain-gut axis homeostasis),[28] and interleukin-6 (IL-6; inflammation marker)[29]; fecal samples were analyzed for α-1-antitrypsin (intestinal permeability)[30] and stool consistency.[23] After euthanasia, brain tissues containing the ACC (key representative region among the multifocal neurophenotype signatures identified by human MRI) were collected, and analyzed for c-Fos (neuronal activation marker),[31] as well as for indoleamine 2,3-dioxygenase 1 (IDO1; a key tryptophan-metabolizing enzyme)[32] and 5-hydroxytryptamine (5-HT; a downstream effector of the tryptophan pathway)[32]; and colonic tissues were evaluated for inflammation using hematoxylin and eosin (H&E) staining (Supporting Information S1). Comparative analysis of brain-gut axis indicators was used to validate the therapeutic potential of neurophenotypes.

2.6 | Statistical analysis

Statistical analyses were performed using R statistical software. Univariate analysis was performed using Student's *t* test, Mann-Whitney *U* test, or Chi-square test according to data distribution. Correlation analyses used Pearson or Spearman methods. Other statistical methods

are described in the corresponding sections of the main text or supplementary materials. A two-sided p-value < 0.050 indicated statistical significance, while a p-value < 0.1 represented marginal significance. Benjamini-Hochberg correction was applied to multiple comparisons of microbiota and metabolomes, with significance defined as False Discovery Rate (FDR) < 0.1.

3 | RESULTS

3.1 | Multimodal neuro-MRI identifies distinct CD neurophenotypes

We used machine-learning approach to extract 13,870 multimodal neuro-MRI features from the training cohort (Figure 1A). Feature selection prioritized 13 discriminative biomarkers (4 neural activity loci, 9 microstructural loci) for developing a neurophenotype characterization model (Figure 1B, Supporting Information S1: Table S2). SHAP analysis revealed their directional contributions to neurophenotype classification (weights: 0.115–0.640; Figure 1C).

The model effectively distinguished neural signatures between CD patients with different intestinal inflammation severity (training cohort, AUC = 0.842, 95% confidence interval [CI], 0.756–0.921; validation cohort, AUC = 0.815, 95% CI, 0.707–0.900). External testing confirmed its cross-center reproducibility (AUC = 0.824, 95% CI, 0.652–0.961; Figure 1D, detailed performance metrics such as sensitivity and specificity are shown in Supporting Information S1: Table S3). SHAP force plots illustrated the neural signature characterization process (Figure 1E). An optimized neurophenotype score threshold (0.45) stratified patients into distinct subgroups. Moreover, HCs showed lower neurophenotype scores than CD patients (0.21 ± 0.14 vs. 0.48 ± 0.31, $p < 0.001$), confirming the model's specificity for CD.

Neurophenotype scores correlated with baseline inflammation severity (MaRIA, $r = 0.41$, $p < 0.001$, Figure 1F; MEGS, $r = 0.38$, $p < 0.001$, Figure 1G) in all 109 patients. Patients with moderate-to-severe inflammation exhibited higher neurophenotype scores than those with no-to-mild inflammation ($p < 0.001$; Figure 1H). Moreover, depression severity (BDI scores) correlated with neurophenotype scores ($r = 0.250$, $p = 0.009$) and intestinal inflammation (MaRIA, $r = 0.26$, $p = 0.006$; MEGS, $r = 0.31$, $p = 0.001$) (Supporting Information S1: Figure S2), while other psychological traits showed no inflammation-dependent differences (all $p > 0.05$).

Overall, multimodal MRI-derived neurophenotypes capture brain-gut axis dysregulation in CD patients, providing an objective framework for neural subtyping and stratification.

3.2 | High-risk neurophenotype links to CD progression independent of intestinal inflammation

After establishing neurophenotype characterization, we investigated their impact on disease progression in 83 follow-up patients (26 progressed; male/female = 23/3). At baseline, patients were divided into four groups based on neurophenotype scores and intestinal inflammation: Group 1 (no-to-mild inflammation with neurophenotype score <0.45, $n = 37$), Group 2 (no-to-mild inflammation with neurophenotype score ≥0.45, $n = 10$), Group 3 (moderate-to-severe inflammation with neurophenotype score <0.45, $n = 8$), and Group 4 (moderate-to-severe inflammation with neurophenotype score ≥0.45, $n = 28$). Among patients with comparable intestinal inflammation, those harboring neurophenotype scores ≥0.45 exhibited higher progression rates: 40.0% versus 13.5% ($p = 0.151$) in no-to-mild inflammation (Group 2 vs. 1), 57.1% versus 12.5% ($p = 0.067$) in moderate-to-severe groups (Group 4 vs. 3; Figure 2A). These findings defined neurophenotype score ≥0.45 as "high-risk" and <0.45 as "low-risk".

Longitudinal assessment revealed diverging trajectories between neurophenotypes and intestinal inflammation. Mean neurophenotype scores and BDI increased while intestinal inflammation (MaRIA/MEGS) decreased (Supporting Information S1: Figure S3). 100% (6/6) of baseline high-risk neurophenotypes persisted in a repeated neuro-MRI subset, while 16.7% (1/6) of them shifted intestinal inflammation categories (Figure 2B). Neurophenotype scores showed no correlation with follow-up inflammation severity (MaRIA/MEGS, $r = 0.17$–0.18, both $p > 0.50$). Depression assessment (BDI scores) mirrored this pattern: 82.35% (28/34) maintained baseline depression, while 35.29% (12/34) exhibited intestinal inflammation fluctuations (Figure 2C), with no BDI-inflammation correlation (MaRIA/MEGS, both $r = 0.18$, $p > 0.10$). These findings indicated that high-risk neurophenotype and associated depression may influence disease progression independently of intestinal inflammation.

Multivariate Cox regression adjusted for baseline intestinal inflammation and clinical factors identified high-risk neurophenotype as the strongest independent predictor (hazard ratio [HR] = 15.46, $p = 0.030$; Table 2), followed by BDI scores (HR = 1.04, $p = 0.040$). Progressors exhibited higher baseline neurophenotype scores than non-progressors ($p < 0.001$; Figure 2D). A neurophenotype-based logistic regression model for predicting progression achieved 5-fold cross-validated rocAUC of 0.74 (95% CI, 0.691–0.787; Figure 2E; Supporting Information S2). High-risk neurophenotype

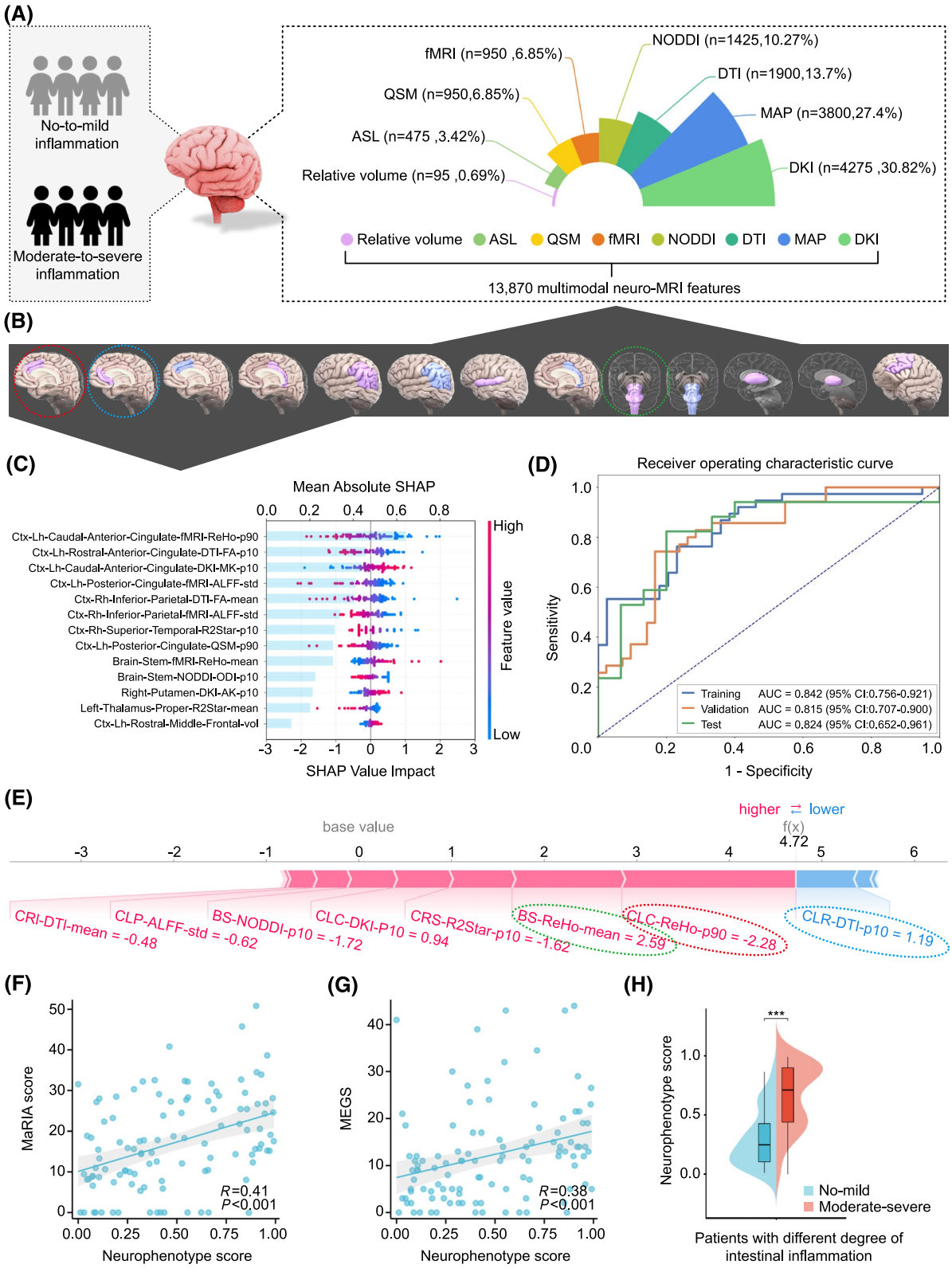

FIGURE 1 Legend on next page.

patients had shorter disease-progression-free survival than low-risk patients ($p < 0.001$; Figure 2F), consistent across inflammation subgroups (no-to-mild, $p = 0.062$; moderate-to-severe, $p = 0.060$; Figure 2G–H).

Neurophenotype scores positively correlated with five key intestinal remodeling features: mural T2WI-hyperintensity, contrast-enhanced pattern, peri-enteric effusion, comb sign (all $p < 0.05$), and wall thickening

($p < 0.10$; Supporting Information S1: Figure S4A). These MRE features further correlated with disease progression (all $p < 0.05$, except mural T2WI-hyperintensity [$p = 0.094$]; Supporting Information S1: Figure S4B). An MRE-feature-integrated logistic regression model predicting disease progression achieved 5-fold cross-validated rocAUC of 0.69 (95% CI, 0.584–0.798; Supporting Information S1: Figure S4C; Supporting Information S2).

Overall, a high-risk neurophenotype is associated with disease progression through intestinal remodeling independent of intestinal inflammation. Its relative stability contrasts with intestinal inflammation volatility and positions the brain-gut axis as central to disease trajectories. These findings imply a high-risk neurophenotype as a durable pathogenic factor rather than an epiphenomena, offering a novel therapeutic target beyond conventional anti-inflammatory strategies.

3.3 | Using multi-omics to investigate mechanisms of high-risk neurophenotype-driven progression

To investigate this brain-gut interaction mechanisms, we integrated neurophenotype scores with fecal microbiome (Supporting Information S3, S4), targeted blood/fecal metabolome (Supporting Information S5, S6), targeted blood neurotransmitters (Supporting Information S7), intestinal remodeling features, and clinical outcomes.

3.3.1 | High-risk neurophenotype contributes to disease progression via modulating gut microbiota and metabolites

We first assessed alpha and beta diversity to characterize the overall gut microbial composition. No significant differences were observed between high-risk and low-risk neurophenotype groups in either alpha diversity or beta diversity analyses (Supporting Information S1: Figure S5). Therefore, to identify specific gut microbiota signatures linked to neurophenotypes, we further combined Linear discriminant analysis Effect Size (LEfSe; Figure 3A) and correlation analyses with four feature selection methods including Least absolute shrinkage and selection operator (LASSO, Figure 3B), Boruta (Figure 3C), Random Forest Recursive Feature Elimination (RF-RFE) and Random Forest Feature (RFF). Consensus across these methods revealed 15 (16S rRNA amplicon sequencing) and 56 (metagenomics) significantly different taxa (Supporting Information S1: Figure S6A-B; ≥ 2 methods), and 8 and 10 strikingly significant differential bacteria (Figure 3D; ≥ 3 methods). Despite differences in bacterial taxa precision identification, these two sequencing approaches consistently detected significant associations between the relative abundance of *Enterococcus*, *Rothia*, *Streptococcus*, *Coprococcus*, *Actinomyces*, *Ruminococcus* and their corresponding species with patient neurophenotypes (Supporting Information S1: Figure S6A,B). Most of these bacteria play

FIGURE 1 Multimodal neuro-MRI identifies distinct neurophenotypes in CD patients. (A) Multimodal neuro-MRI feature extraction (13,870 parameters) from 109 CD patients with different intestinal inflammation severity recruited from two centers (no-to-mild inflammation, $n = 54$, moderate-to-severe inflammation, $n = 55$). (B) Three-step feature selection strategy identifies 13 neurophenotype biomarkers, with associated brain regions highlighted (purple/blue). (C) SHAP analysis quantifies 13 directional feature contributions to neurophenotype classification (rightward shift: high-risk prediction; leftward: low-risk). Color gradient reflects the parameter magnitude (red: high; blue: low). (D) The model distinguishes neural signatures in CD patients with different intestinal inflammation across two centers (Center 1, $n = 77$; Center 2, $n = 32$). (E) SHAP force plot demonstrates model-derived neural signatures in a representative patient, with three key neurophenotype features (green/red/blue) aligning with corresponding brain regions in (B). (F, G) Neurophenotype scores correlate with baseline intestinal inflammation severity ($n = 109$). (H) Patients with moderate-to-severe intestinal inflammation ($n = 55$) exhibit higher neurophenotype scores than those with no-to-mild inflammation ($n = 54$). (Brain-Stem-NODDI-ODI-p10, Brain Stem-Neurite Orientation Dispersion and Density Imaging-Orientation Dispersion Index-10th Percentile [BS-NODDI-p10]; CD, Crohn's disease; Ctx-Lh-Caudal-Anterior-Cingulate-DKI-MK-p10, Cortex-Left Head-Caudal Anterior Cingulate-Diffusion Kurtosis Imaging-Mean Kurtosis-10th Percentile [CLC-DKI-p10]; Ctx-Lh-Caudal-Anterior-Cingulate-fMRI-ReHo-p90, Cortex-Left Head-Caudal Anterior Cingulate-functional MRI-Regional Homogeneity-90th Percentile [CLC-ReHo-p90]; Ctx-Lh-Posterior-Cingulate-fMRI-ALFF-std, Cortex-Left Head-Posterior Cingulate-functional MRI-Amplitude of Low-Frequency Fluctuations-Standard Deviation [CLP-ALFF-std]; Ctx-Lh-Posterior-Cingulate-QSM-p90, Cortex-Left Head-Posterior Cingulate-Quantitative Susceptibility Mapping-90th Percentile; Brain-Stem-fMRI-ReHo-mean, Brain Stem-functional MRI-Regional Homogeneity-Mean [BS-ReHo-mean]; Ctx-Lh-Rostral-Anterior-Cingulate-DTI-FA-p10, Cortex-Left Head-Rostral Anterior Cingulate-Diffusion Tensor Imaging-Fractional Anisotropy-10th Percentile [CLR-DTI-p10]; Ctx-Lh-Rostral-Middle-Frontal-vol, Cortex-Left Head-Rostral Middle Frontal-Volume; Ctx-Rh-Inferior-Parietal-DTI-FA-mean, Cortex-Right Head-Inferior Parietal-Diffusion Tensor Imaging-Fractional Anisotropy-Mean [CRI-DTI-mean]; Ctx-Rh-Inferior-Parietal-fMRI-ALFF-std, Cortex-Right Head-Inferior Parietal-functional MRI-Amplitude of Low-Frequency Fluctuations-Standard Deviation; Ctx-Rh-Superior-Temporal-R2Star-p10, Cortex-Right Head-Superior Temporal-Transverse Relaxation Rate (R2*)-10th Percentile [CRS- R2Star-p10]; Left-Thalamus-Proper-R2Star-mean, Left Thalamus Proper-Transverse Relaxation Rate (R2*)-Mean; MRI, magnetic resonance imaging; Right-Putamen-DKI-AK-p10, Right Putamen-Diffusion Kurtosis Imaging-Axial Kurtosis-10th Percentile; SHAP, SHapley Additive exPlanations).

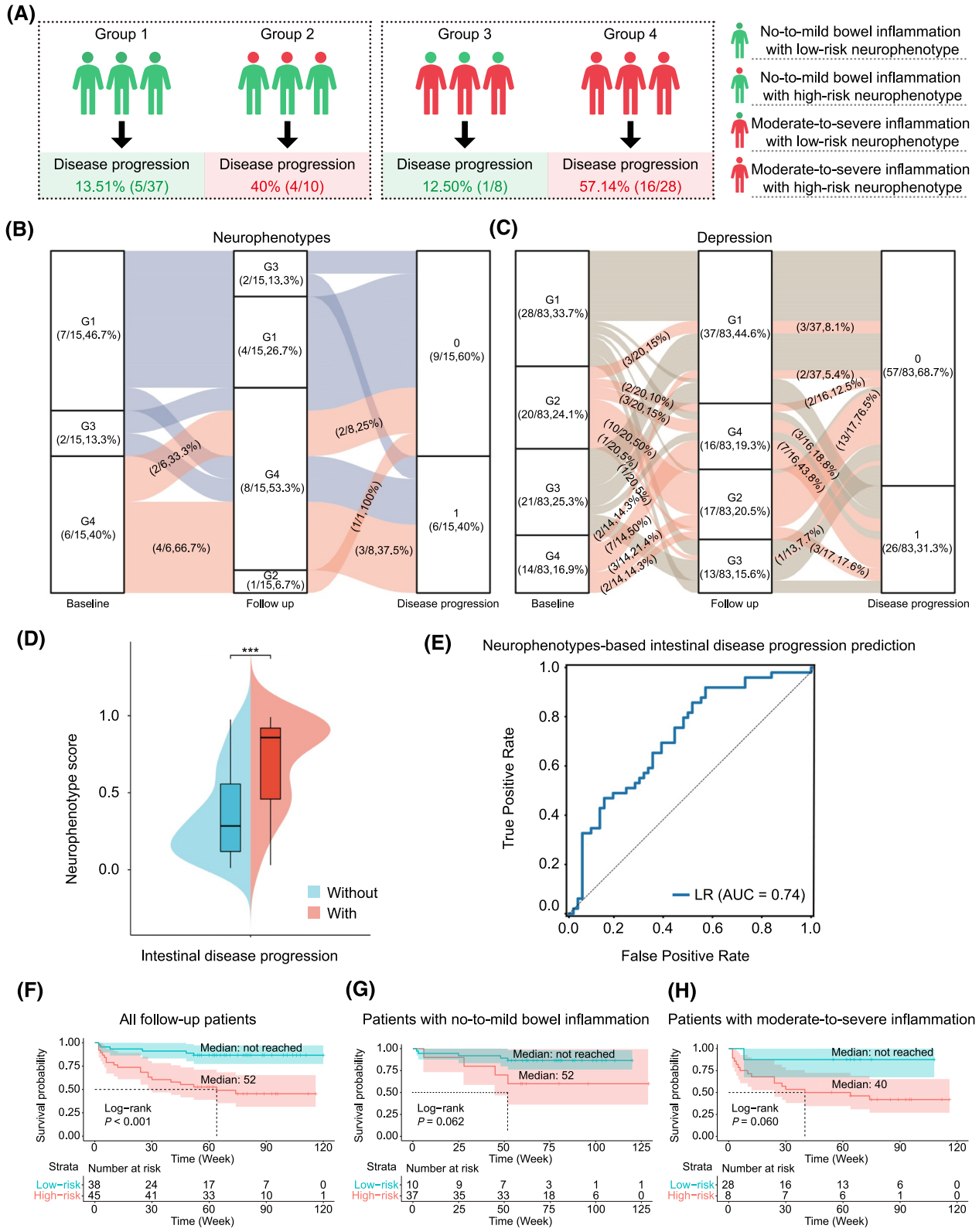

FIGURE 2 Legend on next page.

an important role in CD onset and progression,[33,34] while we first linked them to neurological changes in CD patients. Random forest models trained on these 16S rRNA or metagenomic taxa features achieved satisfactory neurophenotype classification, with 5-fold cross-validated rocAUC of 0.79 (95% CI, 0.622–0.955) and 0.87

TABLE 2 Univariate and multivariate Cox proportional hazard analysis of baseline factors for predicting intestinal disease progression.

Characteristics	Total cohort (n = 83) Hazard ratio (95% CI)	p value
Univariate Cox proportional hazard analysis		
Neuroimaging factor		
Neurophenotype score	20.43 (4.96, 84.21)	<0.001[a]
Psychological scales		
S-score	1.03 (0.99, 1.08)	0.133
T-score	1.03 (0.99, 1.07)	0.145
BDI	1.04 (1, 1.07)	0.038[a]
PSS	1.00 (0.95, 1.05)	0.969
Clinical factors		
Age	1.05 (1.00, 1.10)	0.076
Sex	0.61 (0.18, 2.04)	0.419
BMI	0.90 (0.79, 1.02)	0.108
Smoking history	3.04 (1.14, 8.11)	0.026[a]
Alcohol history	0.72 (0.22, 2.41)	0.595
Education	0.89 (0.60, 1.33)	0.574
Disease duration	1.00 (0.99, 1.01)	0.643
Disease location	1.47 (0.76, 2.84)	0.254
Disease behavior	1.44 (0.82, 2.54)	0.205
Abdominal pain score	0.93 (0.79, 1.10)	0.407
Intestinal inflammation scores		
Intestinal inflammation degree	2.91 (1.29, 6.54)	0.010[a]
Multivariate Cox proportional hazard analysis		
Neurophenotype score	15.46 (1.31, 182.25)	0.030[a]
BDI	1.04 (1.00, 1.09)	0.040[a]
Smoking history	2.01 (0.59, 6.88)	0.263
Intestinal inflammation degree	0.74 (0.17, 3.25)	0.688

Abbreviations: BDI, beck depression inventory; BMI, body mass index; PSS, perceived stress scale; S-score, state score of State-Trait Anxiety Inventory; T-score, trait score of State-Trait Anxiety Inventory.

$p < 0.050$ was considered statistical significance for univariate and multivariate Cox proportional hazard analysis.

[a]Indicates values with significant differences in the univariate and multivariate Cox proportional hazards analysis.

FIGURE 2 High-risk neurophenotype links to CD progression independent of intestinal inflammation. (A) Higher intestinal disease progression rates in high-risk neurophenotype patients (neurophenotype score ≥0.45, Groups 2/4) versus low-risk (<0.45, Groups 1/3), independent of baseline inflammation severity (no-to-mild/moderate-to-severe). (B, C) Longitudinal assessments reveal divergent neurophenotypes and intestinal inflammation trajectories. Sankey diagrams depict baseline-to-follow-up group transitions, with 100% high-risk neurophenotype persistence versus 16.7% intestinal inflammation category shifting (neuro-MRI subset, n = 15) (B). Psychological assessment (n = 83) shows similar dynamics: 82.35% depression persistence versus 35.29% inflammation fluctuations (C). Group definitions (G1–G4) align with (A); disease progression status coded as 0 (no)/1 (yes). Line width reflects sample size. (D) Intestinal disease progressors (n = 26) exhibit higher baseline neurophenotype scores than non-progressors (n = 57) (***$p < 0.001$; Bean plot). (E) Neurophenotype-based progression prediction model (logistic regression, 5-fold rocAUC = 0.74). (F–H) Kaplan–Meier survival curve shows that high-risk neurophenotype patients have shorter disease-progression-free survival than low-risk patients (F), consistent across inflammation subgroups (no-to-mild, G; moderate-to-severe, H). (CD, Crohn's disease; MRI, magnetic resonance imaging; rocAUC, areas under the receiver operator characteristic curve).

(95% CI, 0.786–0.960), respectively (Supporting Information S1: Figure S6C; Supporting Information S2). Notably, taxa differing between high-risk and low-risk neurophenotypes partially overlapped with CD progression-associated taxa (Supporting Information S1: Figure S6D), implicating that gut bacteria might be important links in CD progression-related brain-gut crosstalk. However, traditional mediation analysis found no significant single-taxon pathways (neurophenotype→microbiota→disease progression), suggesting that individual taxa may exert subthreshold effects requiring multi-taxa synergy. To address this, PCMA was used. Both 16S rRNA and metagenomics analyses revealed that neurophenotypes promoted disease progression via multi-bacterial composite principal components (PC3 for 16S rRNA and PC9 for metagenomics; Figure 3E). Loadings analysis highlighted key contributors (Supporting Information S8, S9). For 16S rRNA in PC3, *Rothia* and *Actinomyces* contributed positively, while *uncultured Lachnospiraceae* contributed negatively (Figure 3E). In metagenomics PC9, *Rothia mucilaginosa*, *Streptococcus thermophilus*, and *Streptococcus milleri* made positive contributions, while *Streptococcus mitis* and *Streptococcus rubneri* contributed negatively (Figure 3E).

Blood and fecal metabolomics revealed neurophenotype-discriminatory signatures. Integrated supervised comparisons and machine learning identified 50 blood and 21 fecal metabolites distinguishing neurophenotypes (Supporting Information S10, S11). Of the 50 blood metabolites, 46 are host-derived and four are gut-derived, including two bile acids (GLCA-3S and GDCA-3S) and two short-chain fatty acids (caproic acid and propionic acid) (Supporting Information S12). Machine learning models using these blood or fecal metabolites classified neurophenotypes effectively, with 5-fold cross-validated rocAUC of 0.77 (95% CI: 0.696–0.854) and 0.74 (95% CI: 0.648–0.847), respectively (Supporting Information S1: Figure S6E; Supporting Information S2). Functional enrichment linked blood metabolites to either ether lipid metabolism or primary bile acid biosynthesis pathways and fecal metabolites to amino acid metabolism pathways (Supporting Information S1: Figure S6F). Mediation analysis of "Neurophenotype score→metabolite→disease progression" pathways identified blood CE(24:4) as a significant inhibitory mediator and blood 4-Hydroxyproline as a marginal promoter (Figure 3F). PCMA confirmed the role of CE(24:4) in a multi-metabolite pathway (PC33; Figure 3G). No significant fecal metabolite pathways emerged from traditional or PCMA mediation.

PCMA further uncovered multiple significant "microbiota→metabolite→disease progression" pathways (Figure 3H), where neurophenotype-associated taxa (e.g., *Enterococcus*, *Streptococcus mitis* and *Actinomyces naeslundii*) converged on shared metabolite hubs (e.g., blood metabolite PC1) to collectively drive adverse outcomes. Principal component loading analysis further pinpointed the metabolites (e.g., PC(O−40:5) and ePE(40:5) for blood PC1) as critical contributors to these pathways (Figure 3I; Supporting Information S13, S14).

Collectively, these findings demonstrate that a high-risk neurophenotype contributes to CD progression through integrated microbial-metabolic networks, with multi-omics evidence confirming its causal role rather than incidental association.

3.3.2 | Tryptophan emerges as a key mediator linking high-risk neurophenotype to disease progression

Building on established neurotransmitter roles in brain-gut axis communication,[35] we measured 19 blood neurotransmitters in CD patients. Our analysis revealed that tryptophan, *L*-alanine, and kynurenine were significantly correlated with neurophenotype scores (all $p < 0.05$; Supporting Information S1: Figure S7A), with non-significant trends toward lower levels in high-risk groups (Figure 4A). Among them, tryptophan negatively correlated with four MRE features: mural T2WI-hyperintensity, wall thickness, and peri-enteric effusion (all $p < 0.05$), and contrast-enhanced pattern ($p < 0.1$; Supporting Information S1: Figure S7B). We demonstrated a direct association between tryptophan and both neurological and intestinal changes, consistent with its established role in the brain-gut axis.[35] To further test this relationship, we conducted pathway analysis incorporating neurophenotype score, three neurotransmitters, and five MRE features. Mediation analysis identified tryptophan-mediated pathways from neurophenotypes to T2WI-hyperintensity ($P_{ACME} = 0.046$, mediated effect $p = 0.048$) and comb sign ($P_{ACME} = 0.076$, mediated effect $p = 0.1$; Figure 4B–C), while reverse mediation (intestine→tryptophan→neurophenotype) was non-significant (Figure 4C), confirming predominant brain-to-gut signaling. Moreover, patients experiencing disease progression showed lower tryptophan levels than those without progression ($p = 0.12$, Figure 4D).

Tryptophan's gut-modulating effects may involve microbiota interactions. 16S rRNA sequencing revealed its negative correlations with *Bacteroides* and *Mogibacterium*, while positive correlations with *Escherichia-Shigella* and

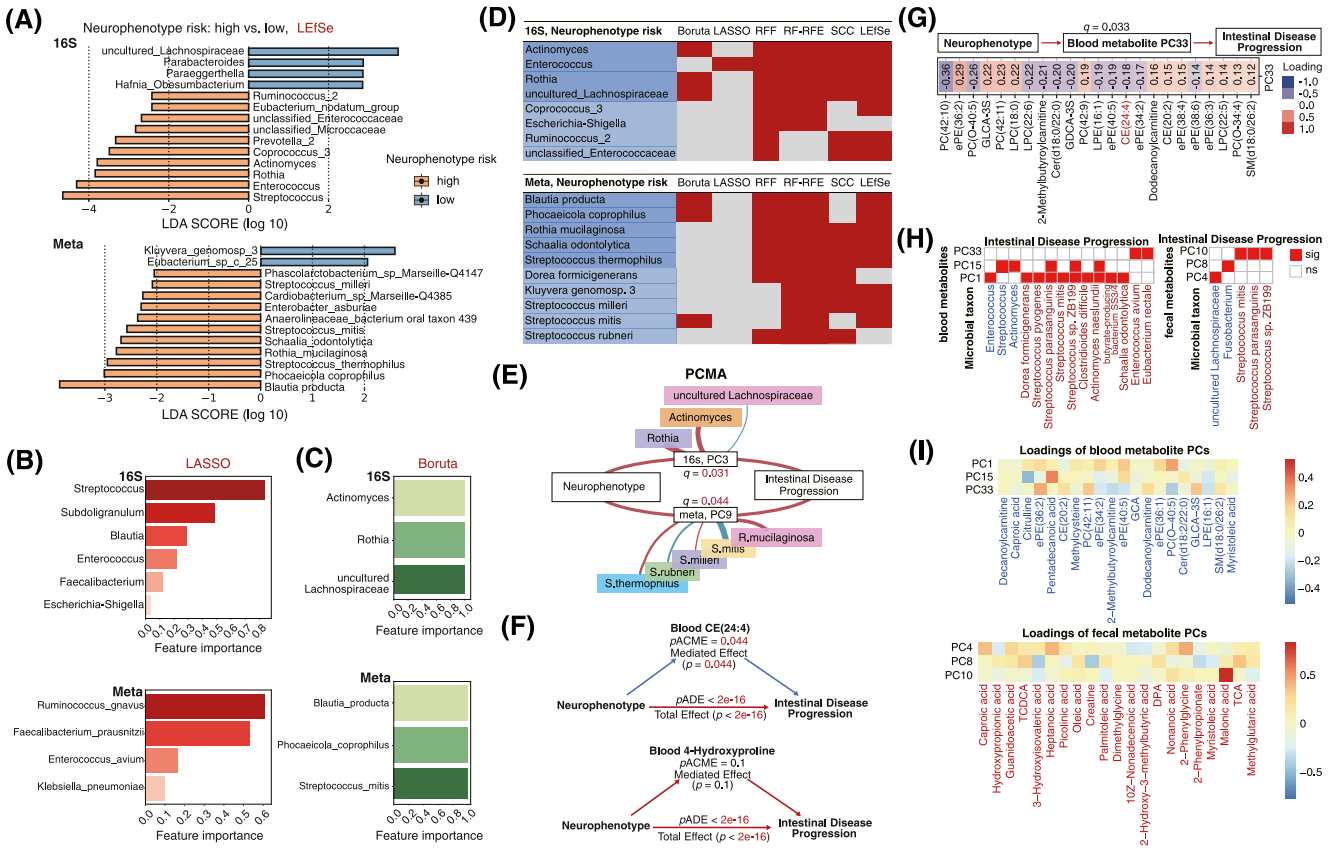

FIGURE 3 High-risk neurophenotype contributes to disease progression via modulating gut microbiota and metabolites. (A–C) Differential gut bacterial taxa between neurophenotype groups identified by LEfSe (A), LASSO (B) and Boruta (C). (D) Consensus bacterial taxa identified across methods (red: significant hits in individual approaches). (E) PCMA-detected significant multi-taxa-mediated pathways connecting neurophenotype and intestinal disease progression, with *q*-values of 0.031 (16S rRNA) and 0.044 (metagenomic) after multiple testing correction (red/blue lines: positive/negative correlations; line width reflects PC3 loadings for taxon contributions). (F) Mediation analysis of neurophenotypes→metabolites→intestinal disease progression (red/blue: positive/negative mediation effects). (G) Principal component loadings for representative blood metabolites in a PCMA-detected significant multi-metabolite-mediated pathway connecting gut bacterial taxa and intestinal disease progression. (H) PCMA-detected significant multi-metabolite-mediated pathways connecting gut bacterial taxa (red:16S rRNA; blue: metagenomic) and intestinal disease progression. (I) Contribution of representative metabolites for PCMA-detected significant multi-metabolite-mediated pathways connecting gut bacterial taxa and intestinal disease progression. The contribution is measured by the PC3 loadings. (LASSO, least absolute shrinkage and selection operator; LEfSe, linear discriminant analysis effect size; RFF, random forest feature; RF-RFE, random forest recursive feature elimination; PCMA, PC3 analysis coupled mediation analysis; PC3, principal component; SCC, spearman correlation coefficient).

Blautia (Figure 4E). Metagenomics expanded these associations: *Lancefieldella parvula*, *Veillonella dispar*, and *Actinomyces graevenitzii* negatively correlated with tryptophan, while *Roseburia intestinalis*, *Bacteroides luhongzhouii*, *Enterobacter roggenkampii*, *Butyrivibrio crossotus*, and *Eubacterium ventriosum* showed positive correlations (Figure 4F). Single-taxon mediation (tryptophan→microbiota→disease progression) was nonsignificant except for *Mogibacterium* detected by 16S rRNA sequencing (P_{ACME} = 0.088), which paradoxically promoted disease progression despite its positive tryptophan association (Figure 4E). Similarly, multi-taxa PCMA analysis identified a significant 16S rRNA-derived pathway (PC4) dominated by *Mogibacterium* (Figure 4G; Supporting Information S15), suggesting coordinated microbial mediation of tryptophan's effects on the gut.

We further conducted pathway analysis on "tryptophan→metabolites→disease progression". Three blood metabolites, glutarylacarnitine, malonic acid, and maltose/lactose, were identified as mediators of the significant effect between tryptophan and disease progression, influencing progression oppositely to tryptophan's direct effect (Figure 4H). While no single fecal metabolite showed significant mediation, a composite fecal

metabolite PC3 was identified as synergistically interacting with tryptophan to inhibit disease progression, in which beta-D-Fucose (+) and Ethylmethylacetic acid (−) played relatively important roles (Figure 4I; Supporting Information S16).

Collectively, tryptophan serves as a key brain-gut axis mediator for reflecting integrated microbial and metabolic network activity and reliably tracking intestinal disease progression during neuro-gut dysregulation. These findings position tryptophan as both a mechanistic link and potential biomarker for monitoring treatment responses in brain-gut axis-targeted interventions.

3.4 | High-risk neurophenotype-targeted neuromodulation alleviates intestinal inflammation in vivo

To evaluate the therapeutic potential of high-risk neurophenotypes, we established DSS-colitis mice and stratified their neurophenotypes into three groups via behavioral experiments (Supporting Information S1: Figure S8): high-risk neurophenotype colitis (G1, $n = 10$), low-risk neurophenotype colitis (G2, $n = 14$), and healthy controls (G3, $n = 15$). Each group contained three subgroups receiving 0, 5, or 10 days of repetitive transcranial

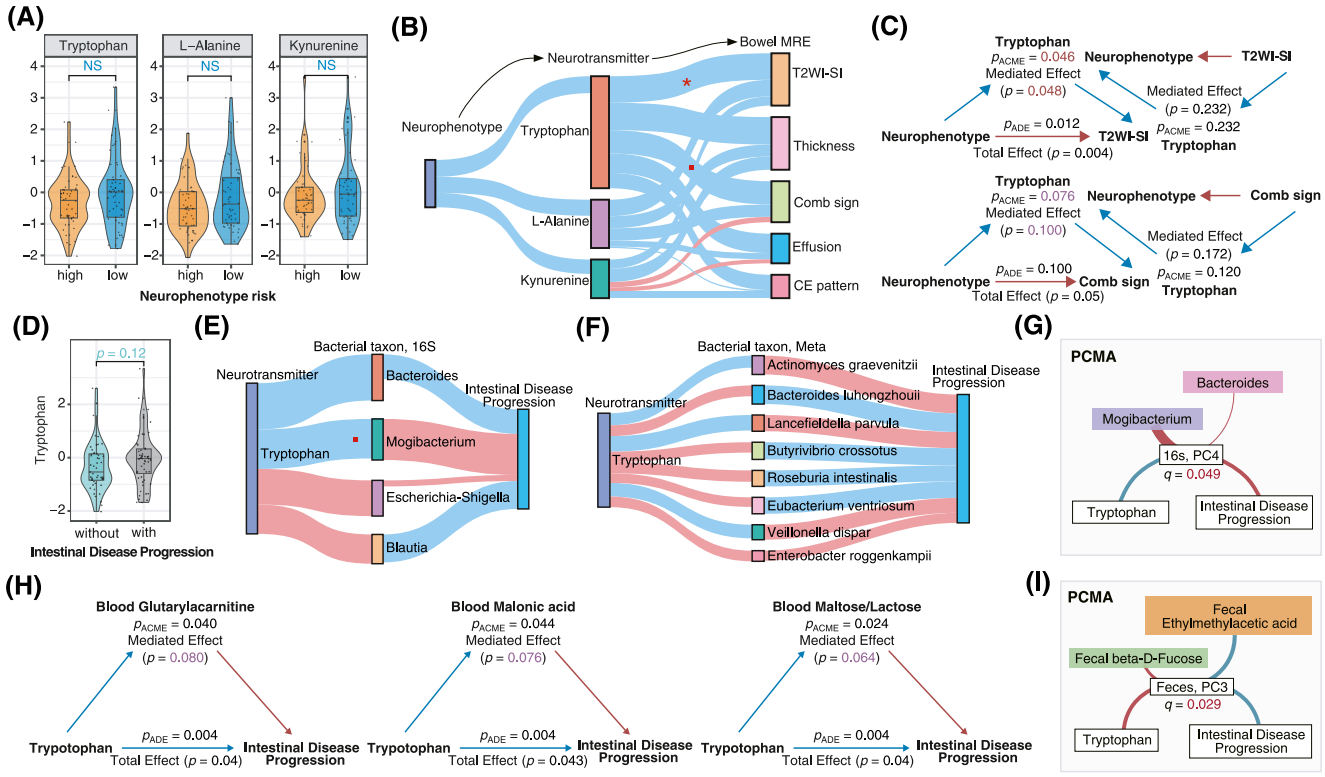

FIGURE 4 Tryptophan emerges as a key mediator linking high-risk neurophenotype to disease progression. (A) Abundance difference of three neurotransmitters between high-risk and low-risk neurophenotypes (Mann–Whitney U test). (B) Sankey diagrams linking neurophenotypes to bowel MRE features via three neurotransmitters using mediation analysis. Red/blue connection lines represent positive/negative correlations. Line width is proportional to the correlation coefficient. *, mediated $p < 0.05$; ●, mediated $p < 0.10$. (C) Bi-directional mediation analysis for "neurophenotype→Tryptophan→bowel MRE" and "bowel MRE→Tryptophan→neurophenotype" pathways. (D) Abundance difference of tryptophan between high-risk and low-risk neurophenotypes (Man–Whitney U test). (E, F) Sankey diagrams connecting neurotransmitters, gut bacterial taxa detected with 16S rRNA sequencing (E) and metagenomic sequencing (F), and intestinal disease progression. Red/blue connection lines represent positive/negative correlations. Line width is proportional to correlation coefficient. ●, mediated $p < 0.10$. (G) A PCMA-detected significant multi-taxa-mediated pathways connecting tryptophan and intestinal disease progression, with a q-value of 0.049 after multiple testing correction (red/blue lines: positive/negative correlations; line width reflects PC3 loadings for taxon contributions). (H) Metabolite-mediated pathways connecting tryptophan and intestinal disease progression detected by mediation analysis. (I) A PCMA-detected significant multi-metabolite-mediated pathways connecting tryptophan and intestinal disease progression, with a q-value of 0.029 after multiple testing correction (red/blue lines: positive/negative correlations; line width reflects PC3 loadings for metabolite contributions). (CE pattern, contrast-enhanced pattern; MRE, magnetic resonance enterography; T2WI-SI, T2-weighted imaging signal intensity; PCMA, PC3 analysis coupled mediation analysis; PC3, principal component).

magnetic stimulation (rTMS) (Figure 5A). Multiple brain-gut axis biomarkers including blood tryptophan were assessed. rTMS, a noninvasive neuromodulation technique, has been widely used for neuropsychiatric disorders[36] and brain-gut axis studies.[37–39] We applied it to address brain-gut dysregulation in our study.

Untreated animals exhibited progressive elevations of neuronal activation marker c-Fos (Figure 5B) and blood-brain barrier damage marker S100β (Figure 5C) from G3 through G2 to G1. rTMS intervention significantly reduced the levels of these markers in G1, with effects increasing over treatment duration. G2 displayed milder baseline abnormalities compared to G1 and also demonstrated reversible neuromodulation effects, whereas G3 showed no significant alterations throughout the treatment period. These findings linked CD neurophenotype severity to neuronal hyperexcitability and blood-brain barrier dysfunction, and demonstrated that rTMS reversed these neuropathological abnormalities by modulating the underlying pathological mechanisms.

Baseline blood tryptophan levels decreased progressively across groups (G3 > G2 > G1), consistent with the trend observed in our CD patient cohort. rTMS intervention significantly restored tryptophan levels in G1, with a time-dependent increase in treatment efficacy. G2 showed a similar improvement, whereas G3 exhibited no significant changes (Figure 5D). Parallel changes were observed in the brain for key upstream metabolic enzymes and downstream effectors of the tryptophan pathway. Brain IDO1 expression increased progressively from G3 to G1, while 5-HT levels exhibited an inverse pattern. rTMS suppressed IDO1 overexpression and rescued serotonin deficits in G1 and G2, but not in G3 (Supporting Information S1: Figure S9). These findings suggested that neurophenotype-targeted treatment can modulate the tryptophan metabolic network and thereby promoted brain-gut axis homeostasis. Concurrently, baseline blood IL-6 levels increased with neurophenotype severity. rTMS induced treatment duration-dependent suppression of IL-6 in G1 and G2 (Figure 5E). This further confirmed that neurophenotype-targeted treatment can drive systemic anti-inflammatory effects.

Critically, neurophenotype-targeted treatment directly ameliorated intestinal inflammation and symptoms. G1 and G2 mice showed varying extents of diarrhea improvement (Supporting Information S1: Figure S10) with enhanced barrier integrity (as evidenced by decreased fecal α-1-antitrypsin levels; Figure 5F) and reduced transmural inflammation (Figure 5G). These treatment duration-dependent gastrointestinal improvements were consistent with the improvement of central nervous system markers (c-Fos/S100β), neurotransmitter (tryptophan), and inflammatory marker (IL-6), further substantiating the causal chain of "neurophenotype-targeted intervention→brain-gut axis remodeling→intestinal repair".

Collectively, our findings demonstrate that correcting the high-risk neurophenotype alleviates colitis, establishing it as an actionable therapeutic target outside the gut. This work provides a mechanistic and therapeutic rationale for moving beyond intestine-centric CD management.

4 | DISCUSSION

The brain-gut axis critically shapes CD pathophysiology, yet the prognostic significance of neurophenotypes and their mechanistic ties to intestinal disease progression remain unresolved. Our study bridges this gap through four key advances. We demonstrated that multimodal neuroimaging can identify distinct CD neurophenotypes by stratifying high-risk and low-risk subgroups with cross-center validity. High-risk neurophenotype exhibited relative stability compared with fluctuating intestinal inflammation, serving as a durable and independent pathogenic factor for disease progression. Multi-omics revealed that a high-risk neurophenotype contributed to CD progression via microbial-metabolic-neurotransmitter networks centered on tryptophan, providing biological evidence to support the high-risk neurophenotype as a promising therapeutic target. We validated this by using rTMS to target high-risk neurophenotype, which elevated tryptophan levels and alleviated colitis in DSS-colitis mice, confirming its therapeutic potential.

Our study redefined neuroimaging characterization of brain-gut interactions in CD. Previous studies predominantly used single or limited MRI modalities to map symptom-associated brain patterns.[5,6,40] By contrast, we extracted 13,870 structural and functional features via multimodal MRI and ultimately distilled 13 biomarkers capturing disease-specific neural signatures. Among them, three top-ranked features were localized to the anterior cingulate cortex, a well-established hub for visceral pain and affective processing in CD,[41] thereby confirming our model's reliability. Moreover, we identified previously unreported microstructural alterations (e.g., inflammation-dependent reductions in brainstem neurite orientation dispersion; Supporting Information S1: Table S2), potentially explaining our model's superior cross-center reproducibility compared to prior studies [5, 6, 40]. These advances resolved the long-standing ambiguity surrounding CD's neural manifestations, enabling stratification into high- and low-risk neurophenotypes using objective neural signatures.

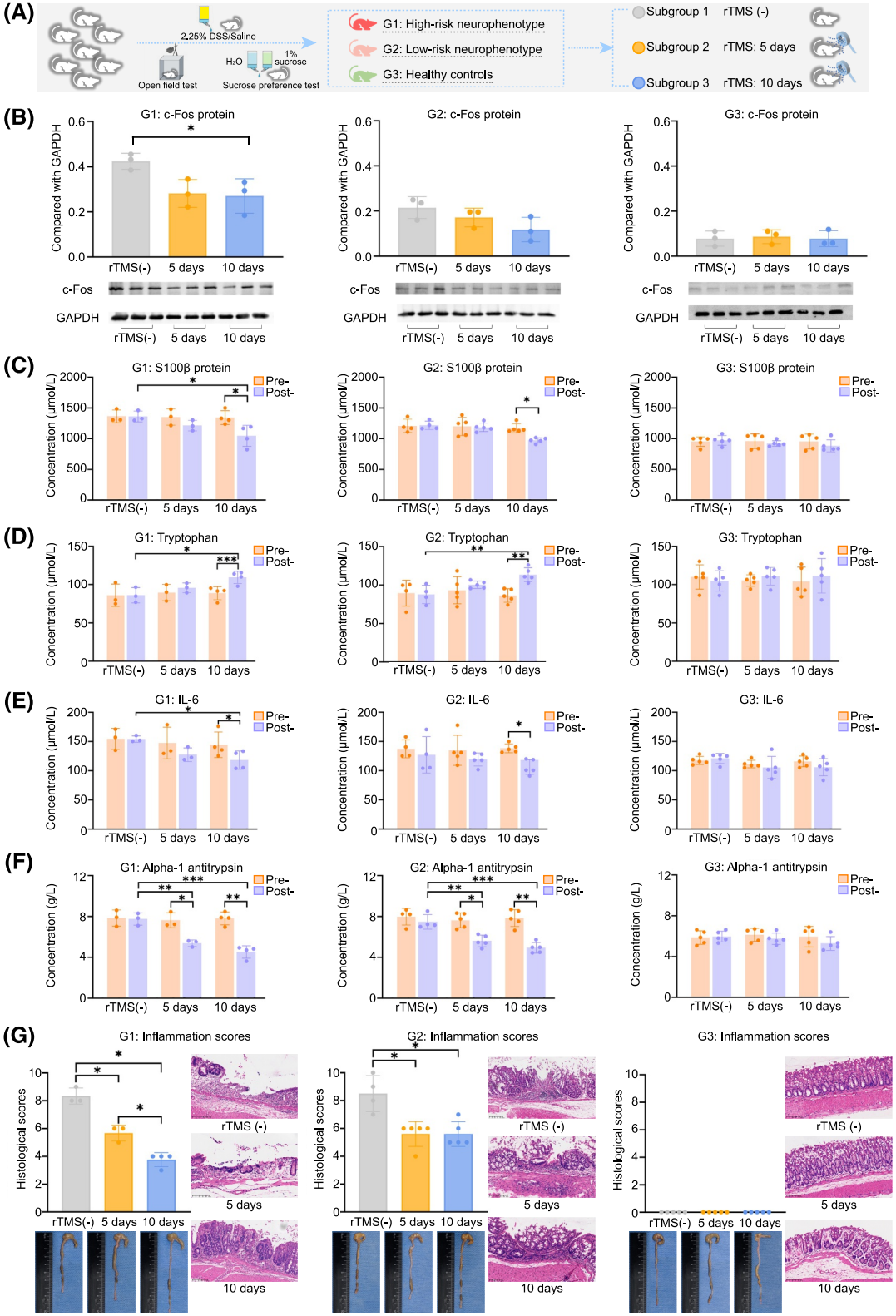

FIGURE 5 Legend on next page.

More importantly, our findings advance our understanding of brain-gut pathogenesis in CD by revealing a high-risk neurophenotype as an independent and durable pathogenic factor for disease progression. While prior studies linked psychological distress to adverse outcomes via self-reported metrics,[3,20] our MRI-based framework

revealed additional insights. First, multimodal MRI-derived neural signatures complemented psychological assessments in progression risk prediction. We further provided evidence that a high-risk neurophenotype may mediate MRE-detectable intestinal remodeling, such as wall thickening and inflammatory congestion, linking it to disease progression. Moreover, the high-risk neurophenotype exhibited relative stability compared with fluctuating gut inflammation, likely due to baseline gut inflammation-driven neuroplasticity that persisted without neural-targeted therapies. Current gut-focused therapies fail to address this neural persistence, leading to a self-reinforcing cycle where high-risk neurophenotype may perpetuate disease progression. This partially explains why some patients treated with the most advanced biologics or small molecules still exhibit suboptimal responses to treatment and supports the emerging management strategy of using neuropsychological-targeted therapies to disrupt pathogenic brain-gut loops.[42]

Our multi-omics analysis demonstrated that the high-risk neurophenotype contributed to CD progression via coordinated microbiota-metabolite-neurotransmitter networks, mechanistically validating its causal role and treatability. Diverging from conventional "gut-to-brain" studies,[43] we systematically mapped "brain-to-gut" pathways using multi-omics data and expanded the above pathogenic cascade: a high-risk neurophenotype disrupts this microecological network balance, induces intestinal remodeling and ultimately advances CD. This hypothesis gained triple support: (1) Neurophenotype-linked microbiota (*Streptococcus/Ruminococcus*) and metabolites (4-hydroxyproline) overlapped with previously reported intestinal remodeling contributors[44,45]; (2) Our mediation analyses confirmed multi-microbial/metabolite networks, rather than isolated components, predominantly mediated neurophenotypic effects; (3) Tryptophan acted as a multi-omics integrator,[28,46] predominantly mediating unidirectional "neurophenotype-to-gut" signaling in our study. This decoded the multi-component interplay in neurophenotype-driven progression while positioning tryptophan as the optimal biosensor for tracking brain-gut axis modulation.

Subsequently, in vivo study established neurophenotype-targeted neuromodulation as a promising therapeutic strategy for CD. In DSS-colitis mice, increased brain c-Fos and serum S100β levels corresponding to escalating neurophenotype severity, implicating neuronal hyperactivation and blood-brain barrier dysfunction involved in high-risk neurophenotype pathogenesis. Neuronal hyperactivation exacerbates colitis while its attenuation improves intestinal inflammation,[47] supporting the feasibility of neurophenotypes as therapeutic targets. Consistent with this notion, after rTMS normalized neural abnormalities, gut-protective effects via brain-gut axis remodeling were observed. Our data revealed that rTMS bidirectionally regulated the central tryptophan metabolic pathway by suppressing IDO1 overexpression and restoring 5-HT levels specifically in a neurophenotype-specific manner. Crucially, changes in serum tryptophan levels with other brain-gut factors pre- and post-intervention validated our multi-omics findings that neurophenotypes modulated tryptophan metabolism and subsequent intestinal alterations. As an important brain-gut mediator, recovered tryptophan may exert systemic benefits through serving as a serotonin precursor regulating enteric neural activity, maintaining mucosal homeostasis via aryl hydrocarbon receptor (AhR) signaling, or suppressing NF-κB-mediated inflammation (evidenced by IL-6 reduction).[48] These mechanisms explained the coordinated improvements in transmural

FIGURE 5 Targeted neuromodulation of high-risk neurophenotype alleviates intestinal inflammation in experimental colitis. (A) Experimental design flowchart for neurophenotype-targeted intervention in DSS-induced colitis models. Experimental timeline before rTMS treatment (DSS: days 1–7; normal water: days 8–10; sucrose preference test: day11; open-field test: day12). (B) Western blot analysis of c-Fos protein expression (neuronal activation marker) in brain tissue containing the anterior cingulate cortex (key representative region among the multifocal neurophenotype signatures identified by human MRI) at the experiment endpoint, with GAPDH as the loading control (rTMS duration: 0/5/10 days; $n = 3$ per subgroup). Western blots were biologically replicated in three samples for each group. Statistical significance was determined by one-way ANOVA analysis. Bars represent mean ± standard deviation. The dots in plots indicate individual mice. $^{*}p < 0.05$. (C–F) Levels of serum S100β protein (C), serum tryptophan (D), serum IL-6 (E) and fecal α-1-antitrypsin (F) pre- versus post-rTMS intervention. Group 1 (subgroups 1–3: $n = 3/3/4$), Group 2 ($n = 4/5/5$), and Group 3 ($n = 5/5/5$). Group and subgroup definitions align with (A). Statistical significance was assessed by paired *t*-tests (within subgroups) and one-way ANOVA (between subgroups). Bars represent mean ± standard deviation. The dots in the plots indicate individual mice. $^{*}p < 0.05$, $^{**}p < 0.01$, $^{***}p < 0.001$. (G) Histological evaluation of intestinal inflammation through H&E staining at the experiment endpoint. Representative colon specimens and associated H&E images for each subgroup are displayed. Group definitions align with (A). Statistical significance of inflammation scores between subgroups was analyzed using Kruskal-Wallis test. Bars represent mean ± standard deviation. The dots in plots indicate individual mice (sample sizes match (C–F) cohorts). $^{*}p < 0.05$. (ANOVA, analysis of variance; DSS, dextran sulfate sodium; GAPDH, glyceraldehyde 3-phosphate dehydrogenase; H&E, hematoxylin and eosin; IL-6, interleukin-6; rTMS, repetitive transcranial magnetic stimulation).

inflammation, barrier function (reduced fecal α-1-antitrypsin), and diarrhea following rTMS. Moreover, the treatment duration-response relationship further confirmed neurophenotype's pathogenic dominance in brain-gut interactions, supporting neural-targeted therapies for some refractory CD. Future studies incorporating comprehensive gut microbiota and serum metabolome profiling in animal models will further elucidate whether neurophenotype-targeted therapies restore the full spectrum of brain-gut metabolic networks.

This study had several limitations. First, the clinical cohort, while double-centered, had a limited sample size, particularly in the neuroimaging follow-up subset, which constrained our ability to assess potential medication effects on neurophenotype stability. Moreover, neurophenotype stratification currently depends on specialized MRI protocols needing technical standardization for broader clinical adoption. Second, the acute DSS-colitis model incompletely mimicked the chronic neuroplasticity progression in CD patients, potentially oversimplifying brain-gut interactions. Therefore, validation in chronic models represents an essential future direction. Third, the multi-omics analyses may be limited by potential biases from unmatched sample collection and the modest cohort size, which could affect the robustness of the findings. Consequently, future validation through longitudinal biospecimen collection with dietary tracking in larger cohorts is warranted. Fourth, we prioritized rTMS over microbiota/tryptophan-targeted interventions (e.g., fecal transplantation, dietary modulation) as rTMS is already widely used in clinical practice, a pragmatic choice enabling more immediate translational potential. Accordingly, exploring these comparative and potentially synergistic approaches represents a promising direction for future brain-gut axis therapeutics in CD. Fifth, our cohort was exclusively Chinese; given that microbiome and metabolome profiles are influenced by regional diet and lifestyle, validation in diverse, multi-ethnic cohorts is essential before global applicability can be established. Additional future directions can include clinical trials for neurophenotype-targeted rTMS treatment in CD patients with extended follow-up to assess the durability of neurophenotype effects, incorporate gender-balanced study designs, extend mechanistic profiling to gut-specific tryptophan metabolites and enzymes, and direct interventional studies to establish causal evidence for the tryptophan pathway in brain-gut axis modulation.

In conclusion, this study establishes a high-risk neurophenotype as both a hallmark extraintestinal manifestation and a persistent driver of CD progression. These findings highlight the critical need for brain-gut axis-targeted therapeutic strategies to advance the precision management of CD.

AUTHOR CONTRIBUTIONS

Study concept and design: Xuehua Li, Ruonan Zhang, Ren Mao and Shi-Ting Feng. *Collecting and analyzing data*: Ruonan Zhang, Xuehua Li, Xiaodi Shen, Shaochun Lin, Zihao Lin, Rongchang Li, Caiguang Liu, Shaochun Lin, Chuhuai Wang, Weikai Zheng, Li Huang, Weitao He, Jinjiang Lin, Haijie Wang and Zhoulei Li. *Drafting manuscript*: Xuehua Li, Ruonan Zhang, Xiaodi Shen. *Critical revision*: Xuehua Li, Ruonan Zhang, Xiaodi Shen, Shaochun Lin, Marietta Iacucci, Subrata Ghosh, Zhenpeng Peng, Canhui Sun, Minhu Chen, Chuhuai Wang, Guang Yang, Yejun Wang, Ren Mao and Shi-Ting Feng. Final approval of manuscript: All authors.

ACKNOWLEDGMENTS

This study was financially supported by National Natural Science Foundation of China (82572164, 82270693, 82471948, 82271958, 82072002, 82070680, and 82222010), Guangdong Basic and Applied Basic Research Foundation (2023B1515020070, 2023A1515011097, and 2026A1515012338), National Key R&D Program of China (2023YFC2507300), Key Area Research and Development Program of Guangdong Province (2023B1111040003), Fundamental Research Funds for the Central Universities, Sun Yat-sen University (24ykqb003), and 2023 SKY Imaging Research Fund of the Chinese International Medical Foundation (Z-2014-07-2301). The funders of the study played no role in study design, data collection, data analysis, data interpretation, or writing of the report.

CONFLICT OF INTEREST STATEMENT

The authors declare no conflicts of interest.

DATA AVAILABILITY STATEMENT

The data that supports the findings of this study are available in the supplementary material of this article.

ETHICS STATEMENT

The human study protocol was approved by the institutional ethics review board of The First Affiliated Hospital of Sun Yat-sen University (No. 2021215-2) with informed consent. The animal experiments received approval from the same institution's Animal Ethics Committee (No. 2023116) and complied with its guidelines. Animals had access to a standard diet and sterile water ad libitum and were housed under controlled temperature, humidity, and a 12-h light/dark cycle.

ORCID

Chuhuai Wang https://orcid.org/0000-0002-8071-9298
Weikai Zheng https://orcid.org/0009-0002-9785-2842
Rongchang Li https://orcid.org/0009-0006-5934-4715
Haijie Wang https://orcid.org/0000-0002-5255-5118
Subrata Ghosh https://orcid.org/0000-0002-1713-7797
Shi-Ting Feng https://orcid.org/0000-0002-0869-7290

REFERENCES

1. J. Torres, S. Mehandru, J. F. Colombel, L. Peyrin-Biroulet, *Lancet* **2017**, *389*, 1741.
2. D. I. Fudman, R. A. McConnell, C. Ha, S. Singh, *Clin. Gastroenterol. Hepatol.* **2025**, *23*, 454.
3. D. J. Gracie, E. A. Guthrie, P. J. Hamlin, A. C. Ford, *Gastroenterology* **2018**, *154*, 1635.
4. D. J. Gracie, P. J. Hamlin, A. C. Ford, *Lancet Gastroenterol. Hepatol.* **2019**, *4*, 632.
5. C. H. Bao, P. Liu, H. R. Liu, L. Y. Wu, X. M. Jin, S. Y. Wang, Y. Shi, J. Y. Zhang, X. Q. Zeng, L. L. Ma, W. Qin, J. M. Zhao, V. D. Calhoun, J. Tian, H. G. Wu, *Pain* **2016**, *157*, 1037.
6. G. Thapaliya, S. Eldeghaidy, M. Asghar, J. McGing, S. Radford, S. Francis, G. W. Moran, *Brain Imaging Behav.* **2023**, *17*, 149.
7. K. A. Knowles, B. O. Olatunji, *Clin. Psychol. Rev.* **2020**, *82*, 101928.
8. S. Cohen, T. Kamarck, R. Mermelstein, *J. Health Soc. Behav.* **1983**, *24*, 385.
9. R. T. Dunn, T. A. Kimbrell, T. A. Ketter, M. A. Frye, M. W. Willis, D. A. Luckenbaugh, R. M. Post, *Biol. Psychiatry* **2002**, *51*, 387.
10. J. Rimola, S. Rodriguez, O. Garcia-Bosch, I. Ordas, E. Ayala, M. Aceituno, M. Pellise, C. Ayuso, E. Ricart, L. Donoso, J. Panes, *Gut* **2009**, *58*, 1113.
11. J. C. Makanyanga, D. Pendse, N. Dikaios, S. Bloom, S. McCartney, E. Helbren, E. Atkins, T. Cuthbertson, S. Punwani, A. Forbes, S. Halligan, S. A. Taylor, *Eur. Radiol.* **2014**, *24*, 277.
12. M. Daperno, G. D'Haens, G. Van Assche, F. Baert, P. Bulois, V. Maunoury, R. Sostegni, R. Rocca, A. Pera, A. Gevers, J. Y. Mary, J. F. Colombel, P. Rutgeerts, *Gastrointest. Endosc.* **2004**, *60*, 505.
13. J. Rimola, I. Ordas, S. Rodriguez, O. Garcia-Bosch, M. Aceituno, J. Llach, C. Ayuso, E. Ricart, J. Panes, *Inflamm. Bowel Dis.* **2011**, *17*, 1759.
14. A. K. Lunder, L. T. Bakstad, J. Jahnsen, A. Borthne, J. R. Hov, M. Vatn, A. Negard, *J. Crohns Colitis* **2019**, *13*, 607.
15. J. C. Makanyanga, S. A. Taylor, *AJR Am. J. Roentgenol.* **2013**, *201*, 56.
16. A. R. Bourgonje, R. Y. Gabriels, M. H. de Borst, M. Bulthuis, K. N. Faber, H. van Goor, G. Dijkstra, *Antioxidants* **2019**, *8*, 351.
17. A. Mohammadi, O. B. Kelly, M. I. Smith, B. Kabakchiev, M. S. Silverberg, *J. Crohns Colitis* **2019**, *13*, 1459.
18. B. Fischl, *Neuroimage* **2012**, *62*, 774.
19. J. Li, S. Liu, Y. Hu, L. Zhu, Y. Mao, J. Liu, *J. Med. Internet Res.* **2022**, *24*, e38082.
20. K. M. Fairbrass, D. J. Gracie, A. C. Ford, *Gastroenterology* **2022**, *163*, 190.
21. W. Kong, Y. Lin, Y. Wang, in *Proceedings of the 15th ACM International Conference on Bioinformatics (BCB '24)*, Association for Computing Machinery, New York, NY, USA **2024**, p. 79.
22. B. Chassaing, J. D. Aitken, M. Malleshappa, M. Vijay-Kumar, *Curr. Protoc. Immunol.* **2014**, *104*, 15.25.1.
23. H. S. Cooper, S. N. Murthy, R. S. Shah, D. J. Sedergran, *Lab. Invest.* **1993**, *69*, 238.
24. F. A. Vicentini, J. C. Szamosi, L. Rossi, L. Griffin, K. Nieves, D. Bihan, I. A. Lewis, Q. J. Pittman, M. G. Swain, M. G. Surette, S. A. Hirota, K. A. Sharkey, *Brain Behav. Immun.* **2022**, *102*, 266.
25. R. Sin, N. Sotogaku, Y. N. Ohnishi, T. Shuto, M. Kuroiwa, Y. Kawahara, K. Sugiyama, Y. Murakami, M. Kanai, H. Funakoshi, A. Chakraborti, J. A. Bibb, A. Nishi, *Brain Behav. Immun.* **2023**, *114*, 173.
26. R. A. Debler, C. A. Madison, L. Hillbrick, P. Gallegos, S. Safe, R. S. Chapkin, S. Eitan, *J. Affect. Disord.* **2023**, *333*, 409.
27. A. A. Kanner, N. Marchi, V. Fazio, M. R. Mayberg, M. T. Koltz, V. Siomin, G. H. Stevens, T. Masaryk, B. Aumayr, M. A. Vogelbaum, G. H. Barnett, D. Janigro, *Cancer* **2003**, *97*, 2806.
28. S. Nikolaus, B. Schulte, N. Al-Massad, F. Thieme, D. M. Schulte, J. Bethge, A. Rehman, F. Tran, K. Aden, R. Hasler, N. Moll, G. Schutze, M. J. Schwarz, G. H. Waetzig, P. Rosenstiel, M. Krawczak, S. Szymczak, S. Schreiber, *Gastroenterology* **2017**, *153*, 1504.
29. R. Atreya, M. F. Neurath, *Clin. Rev. Allergy Immunol.* **2005**, *28*, 187.
30. A. Haidmayer, P. Bosch, A. Lackner, M. D'Orazio, J. Fessler, M. H. Stradner, *Nutrients* **2020**, *12*, 2337.
31. H. D. Mir, Q. Yang, E. Maximin, Q. Montardy, S. Ji, Q. Cheng, X. Shan, L. Wang, L. Naudon, S. Rabot, L. Li, *Neurobiol. Dis.* **2024**, *200*, 106606.
32. Y. Deng, M. Zhou, J. Wang, J. Yao, J. Yu, W. Liu, L. Wu, J. Wang, R. Gao, *Gut Microbes* **2021**, *13*, e1869501.
33. J. D. Forbes, C. Y. Chen, N. C. Knox, R. A. Marrie, H. El-Gabalawy, T. de Kievit, M. Alfa, C. N. Bernstein, G. Van Domselaar, *Microbiome* **2018**, *6*, 221.
34. S. Buffet-Bataillon, G. Bouguen, F. Fleury, V. Cattoir, Y. Le Cunff, *Sci. Rep.* **2022**, *12*, 19929.
35. K. G. Margolis, J. F. Cryan, E. A. Mayer, *Gastroenterology* **2021**, *160*, 1486.
36. A. D. Neacsiu, L. Beynel, J. P. Powers, S. T. Szabo, L. G. Appelbaum, S. H. Lisanby, K. S. LaBar, *Psychother. Psychosom.* **2022**, *91*, 94.
37. G. Li, B. Jin, Z. Fan, *Front. Med.* **2023**, *10*, 1213067.
38. G. Lanza, R. Bella, M. Cantone, G. Pennisi, R. Ferri, M. Pennisi, *Int. J. Mol. Sci.* **2018**, *19*, 2243.
39. K. Jin, B. Chen, S. Han, J. Dong, S. Cheng, B. Qin, J. Lu, *Research* **2024**, *7*, 0384.
40. M. Huang, G. Ma, Y. Zou, H. Ma, W. Fan, X. Li, L. Zhu, P. Han, H. Wang, H. Shi, *Front. Neurosci.* **2024**, *18*, 1361320.
41. N. Kong, C. Gao, M. Xu, X. Gao, *Brain Behav.* **2021**, *11*, e02003.
42. T. H. Bisgaard, K. H. Allin, L. Keefer, A. N. Ananthakrishnan, T. Jess, *Nat. Rev. Gastroenterol. Hepatol.* **2022**, *19*, 717.
43. O. F. Sarb, A. D. Sarb, M. Iacobescu, I. M. Vlad, M. V. Milaciu, L. Ciurmarnean, V. Vacaras, A. I. Tantau, *Int. J. Mol. Sci.* **2024**, *25*, 5676.
44. X. Li, S. Hu, X. Shen, R. Zhang, C. Liu, L. Xiao, J. Lin, L. Huang, W. He, X. Wang, L. Huang, Q. Zheng, L. Wu, C. Sun, Z. Peng, M. Chen, Z. Li, R. Feng, Y. Zhu, Y. Wang, Z. Li, R. Mao, S. T. Feng, *EMBO Mol. Med.* **2024**, *16*, 2427.

45. R. Zhang, Z. Li, L. Huang, W. Kong, Y. Zheng, Y. Wang, X. Shen, L. Huang, X. Wang, Q. Zheng, L. Wu, Y. Ke, R. Mao, Z. Peng, C. Sun, S. Feng, S. Lin, Y. Wang, X. Li, *iScience* **2025**, *28*, 112310.
46. H. Leibovitzh, S. H. Lee, M. Xue, G. J. Raygoza, C. Hernandez-Rocha, K. L. Madsen, J. B. Meddings, D. S. Guttman, O. Espin-Garcia, M. I. Smith, A. Goethel, A. M. Griffiths, P. Moayyedi, A. H. Steinhart, R. Panaccione, H. Q. Huynh, K. Jacobson, G. Aumais, D. R. Mack, M. T. Abreu, C. N. Bernstein, J. K. Marshall, D. Turner, W. Xu, W. Turpin, K. Croitoru, *Gastroenterology* **2022**, *163*, 1364.
47. T. Koren, R. Yifa, M. Amer, M. Krot, N. Boshnak, T. L. Ben-Shaanan, H. Azulay-Debby, I. Zalayat, E. Avishai, H. Hajjo, M. Schiller, H. Haykin, B. Korin, D. Farfara, F. Hakim, O. Kobiler, K. Rosenblum, A. Rolls, *Cell* **2021**, *184*, 5902.
48. C. Xue, G. Li, Q. Zheng, X. Gu, Q. Shi, Y. Su, Q. Chu, X. Yuan, Z. Bao, J. Lu, L. Li, *Cell Metab.* **2023**, *35*, 1304.

SUPPORTING INFORMATION

Additional supporting information can be found online in the Supporting Information section at the end of this article.

How to cite this article: X. Li, R. Zhang, X. Shen, S. Lin, C. Wang, W. Zheng, W. Kong, Z. Lin, R. Li, C. Liu, X. Cao, L. Huang, W. He, J. Lin, H. Wang, Z. Li, M. Iacucci, S. Ghosh, Z. Peng, C. Sun, M. Chen, G. Yang, Y. Wang, R. Mao, S.-T. Feng, *Interdiscip. Med*. **2026**, e70122. https://doi.org/10.1002/inmd.70122